



Antibiotic removal from water: A highly efficient silver phosphate-based Z-scheme photocatalytic system under natural solar light

Jiajia Wang^{a,b}, Hui Chen^{a,b}, Lin Tang^{a,b,*}, Guangming Zeng^{a,b,*}, Yutang Liu^{a,b}, Ming Yan^{a,b}, Yaocheng Deng^{a,b}, Haopeng Feng^{a,b}, Jiangfang Yu^{a,b}, Longlu Wang^c

^a College of Environmental Science and Engineering, Hunan University, Changsha 410082, PR China

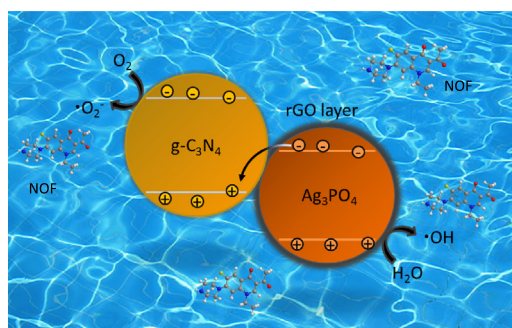
^b Key Laboratory of Environmental Biology and Pollution Control (Hunan University), Ministry of Education, Changsha 410082, PR China

^c State Key Laboratory of Chemo/Biosensing and Chemometrics, Hunan University, Changsha 410082, PR China

HIGHLIGHTS

- A highly efficient and stable Z-scheme photocatalytic system has been successfully constructed.
- AP/rGO/CN composite showed superior photocatalytic performance towards NOF under natural solar light.
- About 85% of NOF can be mineralized after 2 h under natural solar light.
- This Ag_3PO_4 -based Z-Scheme showed good antiphotocorrosion performance.

GRAPHICAL ABSTRACT



ARTICLE INFO

Article history:

Received 27 January 2018

Received in revised form 4 April 2018

Accepted 21 May 2018

Available online xxxxx

Keywords:

Antibiotics removal
Silver phosphate
Z-scheme system
Anti-photocorrosion
Natural solar light

ABSTRACT

Photocatalytic degradation is an alternative method to remove pharmaceutical compounds from water, however it is hard to achieve efficient rate because of the low efficiency of photocatalysts. In this study, an efficient Z-Scheme photocatalyst was constructed by integrating graphitic carbon nitride (CN) and reduced graphene oxide (rGO) with AP via a simple facile precipitation method. Excitedly, ternary AP/rGO/CN composite showed superior photocatalytic and anti-photocorrosion performances under both intense sunlight and weak indoor light irradiation. NOF can be completely degraded in only 30 min and about 85% of NOF can be mineralized after 2 h irradiation under intensive sunlight irradiation. rGO could work not only as a sheltering layer to protect AP from photocorrosion but also as a mediator for Z-Scheme electron transport, which can protect AP from the photoreduction. This strategy could be a promising method to construct photocatalytic system with high efficiency for the removal of antibiotics under natural light irradiation.

© 2018 Elsevier B.V. All rights reserved.

1. Introduction

The increase of antibiotic resistance of microorganism and human body aroused by the abuse of antibiotics in agriculture and healthcare industry raises great public concern (Krumperman et al., 1983; Wong et al., 2000; Tang et al., 2016). Without a good drug supervisory administration, large amounts of the antibiotics released to the environment.

* Corresponding authors at: College of Environmental Science and Engineering, Hunan University, Changsha 410082, PR China.

E-mail addresses: tanglin@hnu.edu.cn (L. Tang), zgming@hnu.edu.cn (G. Zeng).

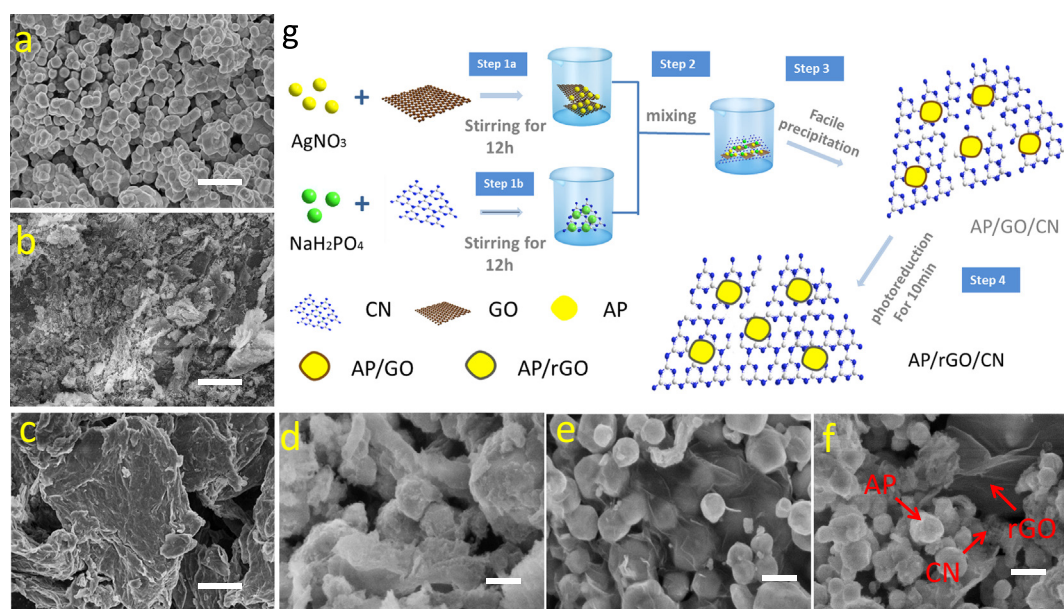


Fig. 1. FESEM images of (a) AP; (b) CN; (c) GO; (d) AP/CN; (e) AP/rGO; (f) AP/rGO/CN composite; and (g) The procedure for the synthesis of AP/rGO/CN composite. The scale bars for a–c and d–f are 2 μm and 200 nm, respectively.

Many of antibiotics detected in aquatic environment, even at trace levels, have been reported to cause antibiotic resistance and have an adverse effect to aquatic wildlife, the ecosystem and human health (Brown et al., 2006; Watkinson et al., 2009; Wang et al., 2017a, 2017b). Thus, the advanced technology for the efficient removal of antibiotics from water should be the focus of our concern.

Semiconductor photocatalysis has been considered to be one of the most promising approaches to remove the organic pollutants especially antibiotics pollutants from water (Hoffmann et al., 1995; Schneider et al., 2014; Tang et al., 2008; Zeng et al., 2013; Yu et al., 2016a, 2016b). However, the low sunlight conversion efficiency is still a big challenge for photocatalysis in practically environmental applications (Deng et al., 2017b; Wang et al., 2017a). Recently, silver based semiconductor photocatalysts including AgX (X = Cl, Br, I) (Wen et al., 2017; Ye et al., 2012), Ag₂CO₃ (Yu et al., 2014), Ag₃PO₄ (Bi et al., 2011), AgVO₃ (Mai et al., 2010), and Ag₂CrO₄ (Deng et al., 2016), have been widely investigated, because they were found as the most efficient visible light response photocatalysts for the removal of organic pollutants. It is

worth noting that Ye et al. fabricated a novel Ag₃PO₄ photocatalyst with extremely high photo-oxidative capabilities for water splitting and organic dye decomposition under visible light irradiation, which achieved the highest quantum efficiency among all existing photocatalysts at wavelength larger than 420 nm (Yi et al., 2010). It could be one of the most promising photocatalyst for practically environmental application. It is noteworthy that Teng's group reported Ag₃PO₄ have a high photoactivity and stability under weak indoor light for the degradation of dye pollutants, which might bring us an achievable technology based on Ag₃PO₄ in water purification (Hua et al., 2015; Teng et al., 2015; Tang et al., 2017). However, Ag₃PO₄ greatly suffers from severe photocorrosion in practical applications because it could decompose rapidly when no sacrificial reagent is involved (Cai et al., 2017; Guan and Guo, 2014; Liu et al., 2016). The biggest obstacle for Ag₃PO₄ in practically application is its severe photocorrosion (Guo et al., 2013; Voiry et al., 2013). Therefore, the key strategy is to inhibit its photocorrosion when it is used in practical application.

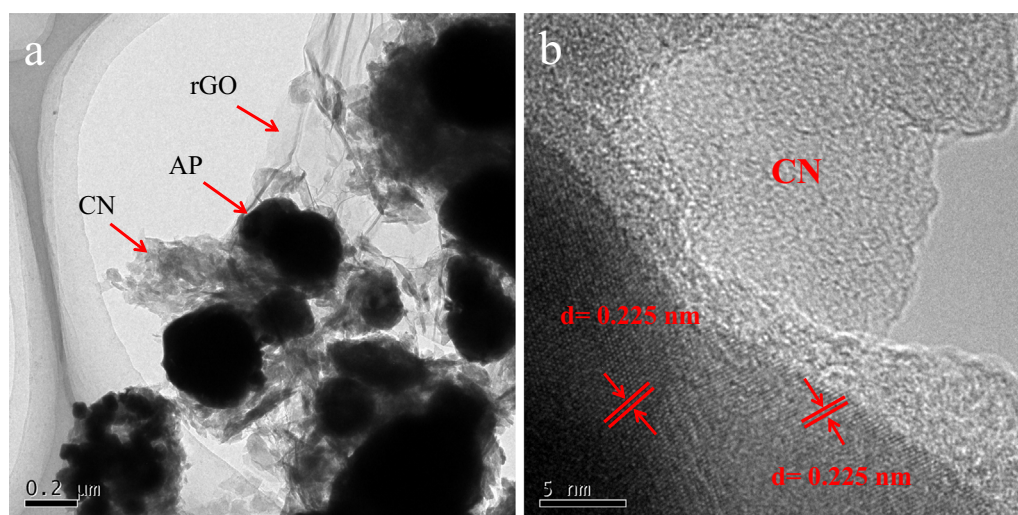


Fig. 2. TEM (a) and HRTEM (b) images of AP/rGO/CN composite.

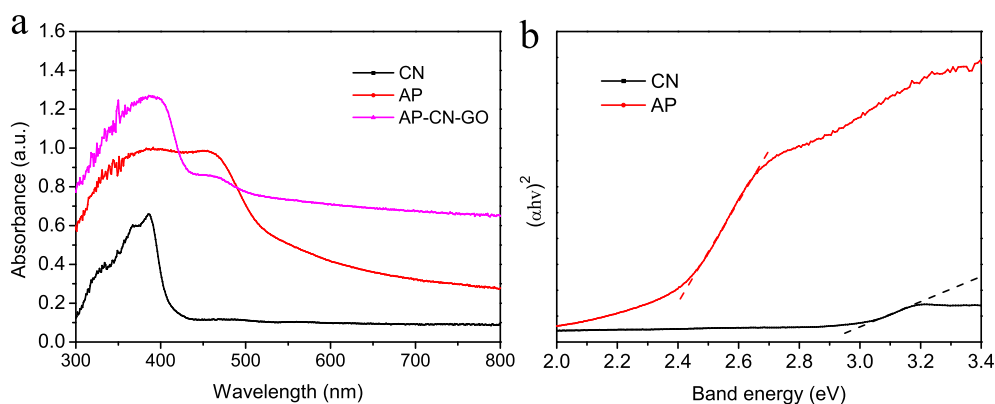


Fig. 3. UV-vis diffuse reflectance spectra of (a) AP, CN, and AP/rGO/CN; (b) Kubelka-Munk curve of different samples.

The main reason for the photocorrosion of Ag_3PO_4 is that Ag^+ can be easily reduced into metal Ag by excited electrons when exposed to light. This could significantly lead to the loss of Ag_3PO_4 and decrease the photocatalytic efficiency of Ag_3PO_4 . Designing silver based photocatalysts with sufficient charge separation efficiency and high anti-photocorrosion performance in the ultraviolet and visible light region is still a big challenge in photocatalysis research. Recently, researchers have tried many methods to strengthen the stable performance of Ag_3PO_4 , including morphology control (Teng et al., 2015; Wang et al., 2012), coupling semiconductor (Hou et al., 2012; Li et al., 2013), and carbon-based composite (He et al., 2014; Liu et al., 2016; Yang et al., 2013). However, the above strategies could not solve the problem essentially and the improvement was relatively small (Li et al., 2016; Wang et al., 2016a). The key to improve anti-photocorrosion performance and photoactivity of Ag_3PO_4 is to consume the electrons or transfer them away timely, thereby avoiding reaction between Ag^+ and electrons.

Inspired by the natural photosynthesis process, the artificial Z-scheme photocatalytic system was proposed and it featured the spatial

isolation of photogenerated electrons and holes, which could reduce the bulk electron-hole recombination (Chen et al., 2017; Sun et al., 2015; Tada et al., 2006). Besides, in Z-scheme heterojunction, photogenerated charges can accumulate on the higher potential energy band rather than transfer to the lower energy band, so that the high potential energy band gets protected, and the electrons and holes can maintain high reactivity. Recently, many Ag_3PO_4 based Z-scheme photocatalytic systems have been proposed, for example, $\text{AgI}/\text{Ag}_3\text{PO}_4$ (Chen et al., 2013), $\text{Ag}_3\text{PO}_4/\text{MoS}_2$ (Wan et al., 2017), $\text{SrTiO}_3/\text{Ag}_3\text{PO}_4$ (Guan and Guo, 2014), $\text{GO}/\text{Ag}_3\text{PO}_4$ (Ao et al., 2013), and $\text{Ag}_3\text{PO}_4/\text{HAp}$ (Chai et al., 2015). Although these Ag_3PO_4 based Z-scheme photocatalytic systems perform efficiently in relaying electrons, a solid electron mediator is more favorable in terms of accelerating the electron transfer rate between two photocatalysts (Deng et al., 2017a; Wang et al., 2016b). The photocatalyst-mediator-photocatalyst contact interface is also very crucial to ensure a continuous flow of electrons between photocatalysts and target pollutants (Zhou et al., 2014).

In this study, we fabricated a well-designed Z-Scheme photocatalysis system composed of reduced graphene oxide-enwrapped Ag_3PO_4 (AP/

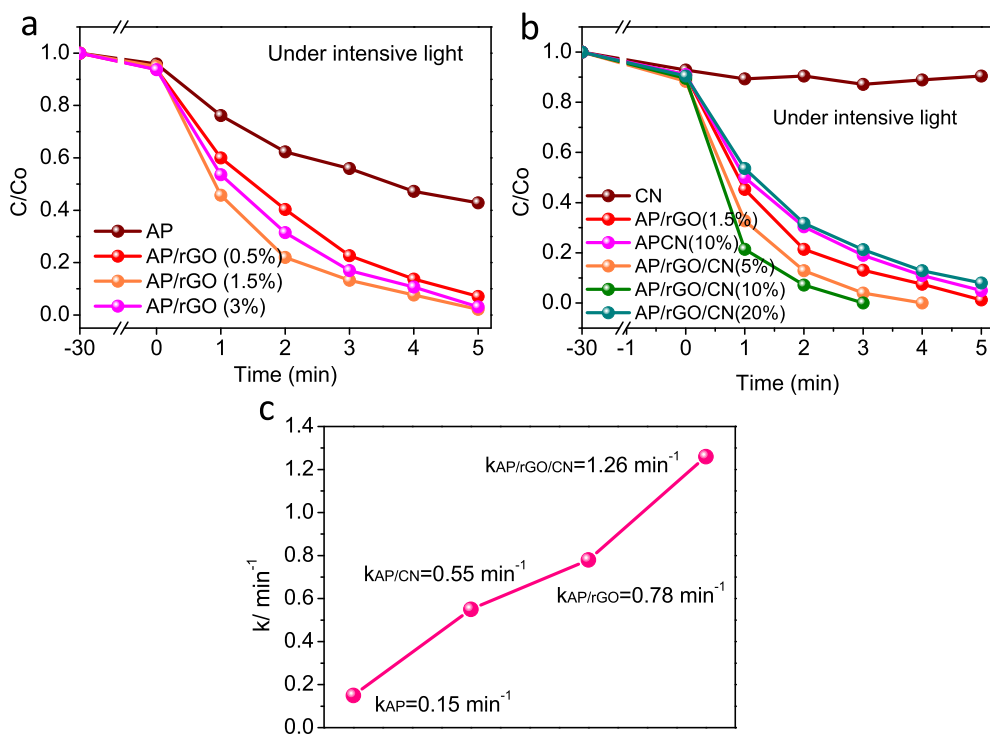


Fig. 4. (a, b) Photodegradation curves of RhB under the intensive sun light irradiation by the as-prepared samples of different mass ratios; (c) reaction kinetic rate of as-prepared samples. $[\text{RhB}] = 10 \text{ mg L}^{-1}$; $[\text{AP}] = 1 \text{ g L}^{-1}$.

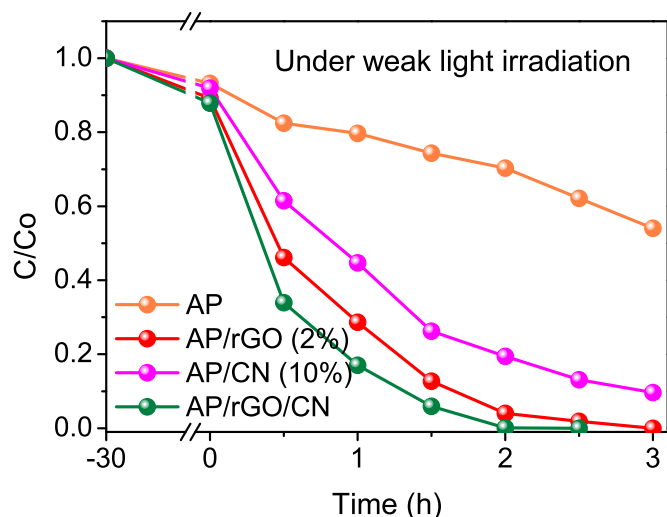


Fig. 5. Photodegradation curves of RhB under weak indoor light irradiation by AP and AP composites. [RhB] = 10 mg L⁻¹; [AP] = 1 g L⁻¹.

rGO) and graphic carbon nitride (g-C₃N₄, CN). Compared with pure Ag₃PO₄ (AP), CN, and the binary composites AP-CN, AP-rGO, the unique ternary Z-Scheme architecture (AP/rGO/CN) displayed obviously enhanced photocatalytic and anti-photocorrosion performances in degradation of norfloxacin (NOF) under natural solar light. It is because the rGO could help electrons efficiently transport from the conduction band (CB) of Ag₃PO₄ to the valence band (VB) of g-C₃N₄, which results in enhanced separation efficiency of electron-hole pairs and the formation of rich-hole region on the surfaces of Ag₃PO₄. This work provides a new application of Z-Scheme photocatalytic system for protection of photosensitive semiconductors from photocorrosion and effective elimination of antibiotic pollutants under the natural solar light irradiation.

2. Experimental

2.1. Chemicals

All chemicals were of analytical grade and without further purification before use. Silver nitrate, sodium hydrogen phosphate, graphite, and melamine were purchased from Sinopharm Chemical Reagent Co. Ltd. All the other reagents were purchased from Shanghai Reagents Company (Shanghai, China).

2.2. Preparation of AP/rGO/CN ternary composite

The detailed fabrication procedure was given in SI.

2.3. Characterization

The morphologies were examined by field emission scanning electron microscopy (FE-SEM) (Hitachi, S-4800) and a transmission electron microscope (TEM, TECNAI G2 F20). UV – vis diffuse reflectance spectra of the photocatalysts were performed on an UV – vis spectrophotometer (Cary 300, USA). The photoluminescence (PL) measurements were carried out on F-7000 at room temperature.

2.4. Photodegradation under intensive solar light

Photocatalytic performance of the as-prepared samples was tested by the degradation of RhB and NOF under natural intensive solar light irradiation. The irradiance was measured and listed at Table S1. Typically, 50 mg of photocatalyst was dispersed into the reaction solution (50 mL, 10 mg L⁻¹ RhB or NOF). The suspension was stirred for 30 min in the darkness to reach an adsorption-desorption equilibrium, and then transferred to the out of the window in our laboratory room (Changsha, China). At a given interval time, 1 mL of suspension was taken out and separated through centrifugation (4000 rpm, 10 min) during the degradation process. The concentration of remained RhB in supernatants was analyzed by a UV–vis spectrophotometer. The residual NOF concentration was detected by an Agilent HPLC Series 1100 (Agilent, Germany) equipped with a UV–vis detector and a Zorbax SB-C18 column (4.6 × 250 mm, 5 μm) (Zhang et al., 2016). The detection wavelength was set at 268 nm and the injection volume was 20 μL. The initial eluent flow rate was 1 mL min⁻¹. Mobile phase A was H₂O and mobile phase B was HPLC grade acetonitrile (with a ratio of 30:70).

2.5. Photodegradation under weak indoor light irradiation

The degradation experiments were also carried out under weak indoor light irradiation. The irradiance was measured and listed at Table S2, while the other conditions are the same as those above.

3. Results and discussion

3.1. Characterizations of as-prepared photocatalysts

The morphology of the as-prepared samples was first characterized by field-emission scanning electron microscopy (FE-SEM). Fig. 1a clearly shows that the pure AP possesses an irregular sphere-like polyhedral morphology with an average diameter ranging from 300 to

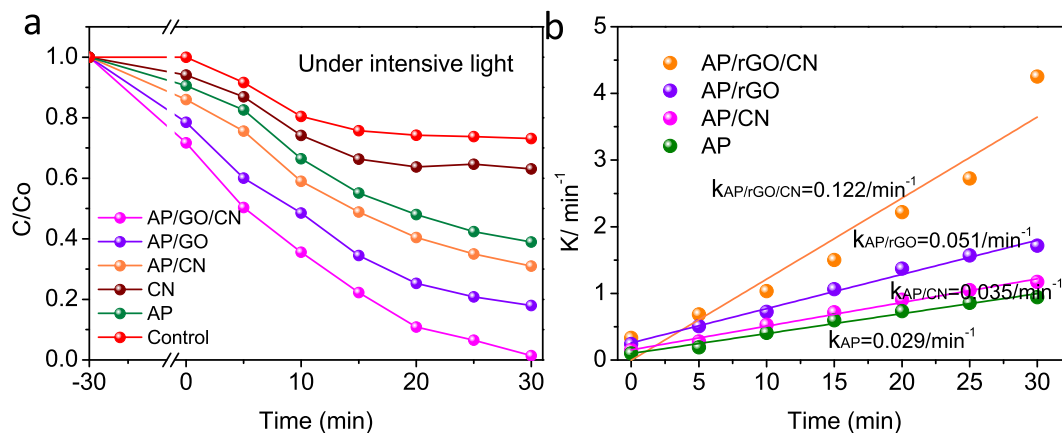


Fig. 6. (a) Photodegradation curves of NOF under the intensive sun light irradiation by AP and AP composites; (b) reaction kinetic curves of AP and AP composites. [NOF] = 10 mg L⁻¹; [AP] = 1 g L⁻¹.

500 nm. Pure CN displays wrinkled lamellar structure with relatively smooth surface (Fig. 1b). Fig. 1c reveals that GO are smooth and crumpled sheets, which was attributed to the deformation and distortion of graphite sheets. It can be seen in Fig. 1d that AP particles are coated with CN and the surface morphology has changed. An FESEM image of AP-rGO composite (Fig. 1e) clearly reveals that it is composed of sphere-like AP polyhedra with an average diameter of ~200 nm, and most particles are wrapped by flexible GO sheets, which implies that the addition of GO has an obvious effect on the morphology of AP particles. For AP/rGO/CN (Fig. 1e), three structures were all found and combined well with each other. Fig. 1g shows the schematic diagram preparation procedure of AP/rGO/CN composite. The TEM and HRTEM characterization were performed by a transmission electron microscope (TEM, TECNAI G2 F20). The typical images of a smooth and wrinkled surface of GO are observed. It can also be clearly seen from Fig. 2a that the Ag_3PO_4 particles with size ranging from 200 to 400 nm are wrapped by CN and rGO, which is consistent with the results of SEM. The corresponding HRTEM image (Fig. 2b) shows clearly that the lattice spacing are 0.268 nm corresponding to the (2 1 0) plane of Ag_3PO_4 . The optical property of AP, CN, and AP/rGO/CN were analyzed by UV–vis diffuse reflectance, and Fig. 3a shows that pure AP and CN exhibited the absorption of sunlight with wavelength shorter than 450 nm. Compared with AP and CN, AP/rGO/CN displays strong absorption in the range of 550–800 nm. The band gap energies of AP and CN can be estimated by Kubelka–Munk transformation, $\alpha h\nu = A(h\nu - E_g)n/2$, where α represents the absorption coefficient, ν is the light frequency, E_g is the band gap energy, A is a constant, and n depends on the characteristics of the transition in a semiconductor. According to Kubelka–Munk transformation, Fig. 3b shows that the E_g values of CN and AP were calculated to be 2.91 and 2.39 eV, respectively.

3.2. Degradation of RhB dye solution

3.2.1. Under outdoor intensive solar light irradiation

The photocatalytic test of AP and its composites towards RhB was conducted under natural intense light irradiation. We first carry out the experiment under the outdoor intensive solar light irradiation out of our laboratory. (Location: Hunan University, N28° 11' 14.26" E112° 57' 6.17"; Date: September 15, 2017; Weather: Sunny day). The optimized mass ratios of the prepared samples were in Fig. 4a and b. In comparison with pure AP, AP/rGO and AP/CN, AP/rGO/CN composites both exhibit superior photocatalytic activities. Surprisingly, the results reveal that the as-prepared samples can efficiently degrade RhB under natural outdoor intense light irradiation. AP/rGO/CN composite shows the highest photoactivity towards RhB, which can completely degrade RhB dye in 3 min (Fig. 4b). The visualized photodegradation experiment for RhB using AP/rGO/CN can be seen in a video (Video 1(SI)). In blank test, self-degradation of RhB was negligible without the addition of catalysts, suggesting the relatively photochemical stability of organic dyes (Fig. 4b). Based on the optimized mass ratios experiment, the optimized mass ratios of rGO and CN towards AP are 1.5% and 10%, respectively. Fig. 4c shows the reaction kinetic parameters of as-prepared samples. The apparent kinetic constants for AP, AP/CN, AP/rGO and AP/rGO/CN composite are 0.15, 0.55, 0.78 and 1.26 min^{-1} , respectively (Fig. 4c). The above results demonstrate that the as-prepared AP/rGO/CN composite can fully and effectively utilize natural light to remove organic pollutants due to the effective band match between CN and AP.

3.2.2. Under natural indoor weak light irradiation

To further test the photocatalytic performance of AP towards RhB under the natural weak indoor light irradiation, we also conducted the photodegradation experiments in our laboratory, in which the irradiance was recorded by radiometer and are presented in Table S2. Amazingly, RhB could also be degraded by AP and its composites under the natural weak indoor light irradiation. AP/rGO/CN composite also shows the highest photoactivity, which can degrade 98% RhB after

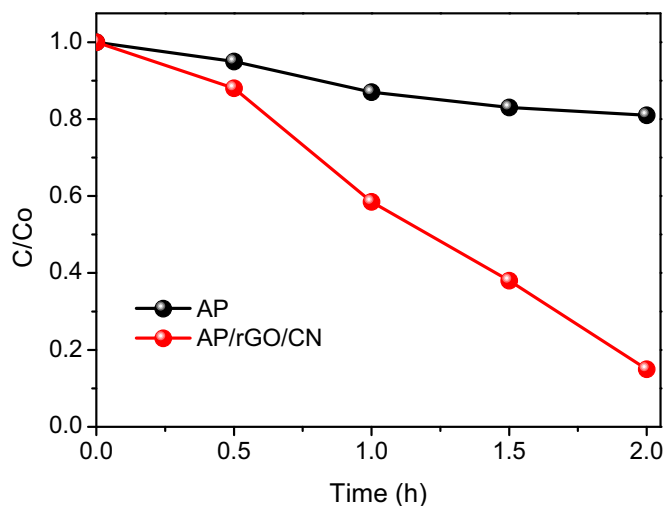


Fig. 7. Mineralization of NOF under the intensive sun light irradiation by AP and AP/rGO/CN composites. $[\text{NOF}] = 10 \text{ mg L}^{-1}$; $[\text{AP}] = 1 \text{ g L}^{-1}$.

exposing to the natural weak indoor light irradiation for 2.5 h (Fig. 5), while only 45% of RhB can be degraded by pure AP in 3 h. The above results show that this ternary AP/rGO/CN composite has wide absorption range and efficient photodegradation efficiency towards RhB under the natural weak light irradiation.

3.3. Degradation of NOF solution

3.3.1. Under natural outdoor intense light irradiation

The photodegradation of NOF by AP and its composites were conducted under outdoor intense light irradiation. Fig. 6a shows that, even without the addition of catalysts, NOF was obviously decomposed under intensive outdoor light irradiation, which might be because the intensive sunlight has ultraviolet light. But compared with the photodegradation of NOF for AP and its composites, photolysis effect is relatively weak. The AP/rGO/CN composite showed an amazingly highest photoactivity towards NOF, which could completely degrade NOF in 30 min. The photodegradation of NOF follows the first order kinetic reaction equation, $-\ln(C/C_0) = kt$, where C_0 and C are the NOF concentrations at time zero and t , respectively, and k is the rate constant. The apparent kinetic constants for AP, AP/rGO, AP/CN and AP/rGO/CN composite are 0.029, 0.051, 0.035 and 0.122 min^{-1} , respectively

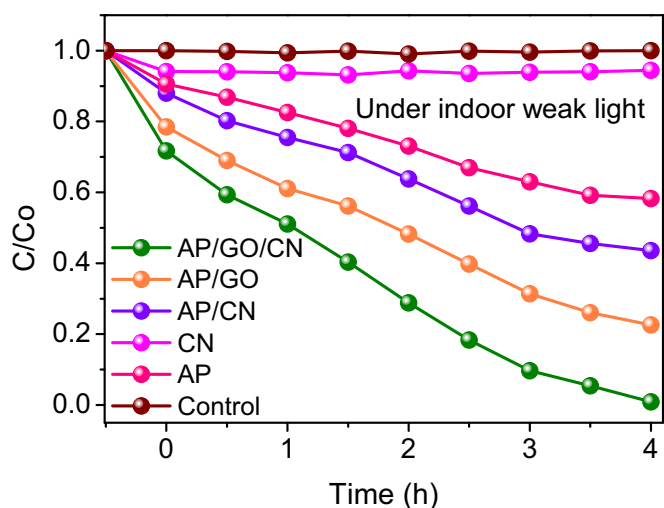


Fig. 8. Photodegradation curves of NOF under weak indoor light irradiation by AP and AP composites. $[\text{NOF}] = 10 \text{ mg L}^{-1}$; $[\text{AP}] = 1 \text{ g L}^{-1}$.

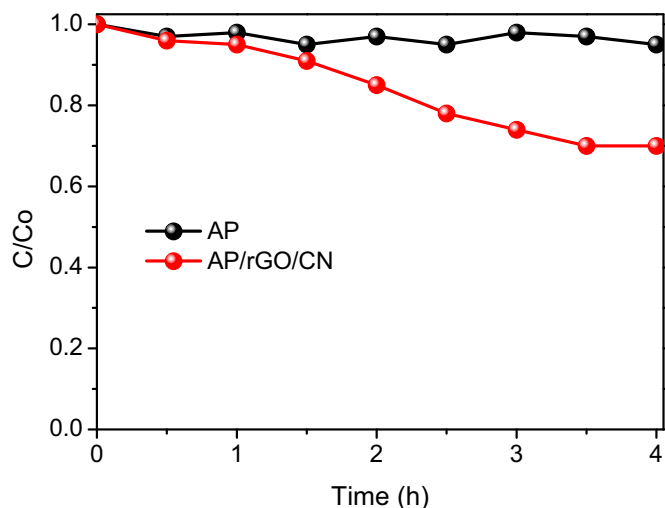


Fig. 9. Mineralization of NOF under weak indoor light irradiation by AP and AP/rGO/CN. [NOF] = 10 mg L⁻¹; [AP] = 1 g L⁻¹.

(Fig. 6b). The above results have demonstrated that AP/rGO/CN composite photocatalytic system could also have excellent activity for the degradation of antibiotic pollutant. Total organic carbon (TOC) was measured with a Shimadzu TOC analyzer (TOC-VCPH). Fig. 7 shows that the TOC value of NOF decreased by ~85.1% after 2 h of outdoor intensive sunlight irradiation, which indicates that NOF mineralization by AP/rGO/CN composite is possible.

3.3.2. Under natural weak indoor light irradiation

The photocatalytic experiments of the as-prepared composites towards NOF were also conducted under the natural weak indoor light irradiation in our laboratory. Amazingly, NOF could also be degraded by AP and its composites under the natural weak indoor light irradiation. AP/rGO/CN composite also showed the highest photoactivity, which could degrade 97% NOF after exposing to the natural weak light irradiation for 4 h (Fig. 8). Fig. 9 shows that the TOC value of NOF decreased by ~30.2% after 4 h, which indicates that NOF mineralized by AP/rGO/CN is possible even under the indoor weak light irradiation. The above results have proved that, although under the natural weak light irradiation, AP/rGO/CN photocatalysis systems have excellent photoactivity for the degradation of antibiotics and dye solution due to its ultra-strong redox ability, relatively high carrier separation efficiency, wide absorption range and unique ternary Z-Scheme architectures.

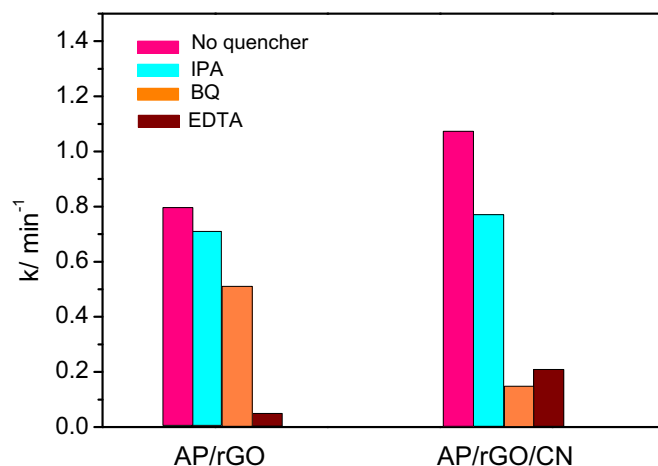


Fig. 11. Photodegradation rates of RhB on AP/rGO and AP/rGO/CN by addition of 10 mM benzoquinone, 10 mM isopropanol, 10 mM EDTA-Na₂. [RhB] = 10 mg L⁻¹; [AP/rGO/CN] = 1 g L⁻¹.

3.4. Photostability and recyclability

The stability of silver based semiconductor photocatalyst is a key issue in practical applications. To investigate the stability of AP and its composites under outdoor intensive light irradiation, the degradation experiments of RhB by as-prepared samples are repeated for 5 cycles. Fig. 10a shows that there is only little loss in the photoactivity for AP/rGO/CN composite after 5 cycles reused. The removal efficiency still remains at 97% in 5 min. However, there is a significant decrease of photocatalytic efficiency for bare AP, which declines by about 31% after 5-cycles reused, because that a large number of AP was greatly reduced into Ag⁰ by photon-generated electrons. With the increase of Ag content, there will be shield silver layer on the surface of AP. The shield layer would block the light absorption of AP, thereby inhibiting the transfer of carriers between AP and solution. To dig deeper to verify the anticorrosive performance for AP/rGO/CN composite, the XRD measurement was employed. The XRD patterns of fresh and used AP and AP/rGO/CN are shown in Fig. 10b. Three peaks emerge at 38.1°, 64.4° and 77.4° for AP sample after 5 cycles, which can be classified as characteristic peaks of silver (JCPDS NO.04-0783) (Yao et al., 2012). Surprisingly, there are no any impurity peak emerged in AP/rGO/CN samples after 5 cycles. Above results powerfully prove that the introduction of rGO and CN was beneficial to solve the photocorrosion problem of pure AP in practical applications.

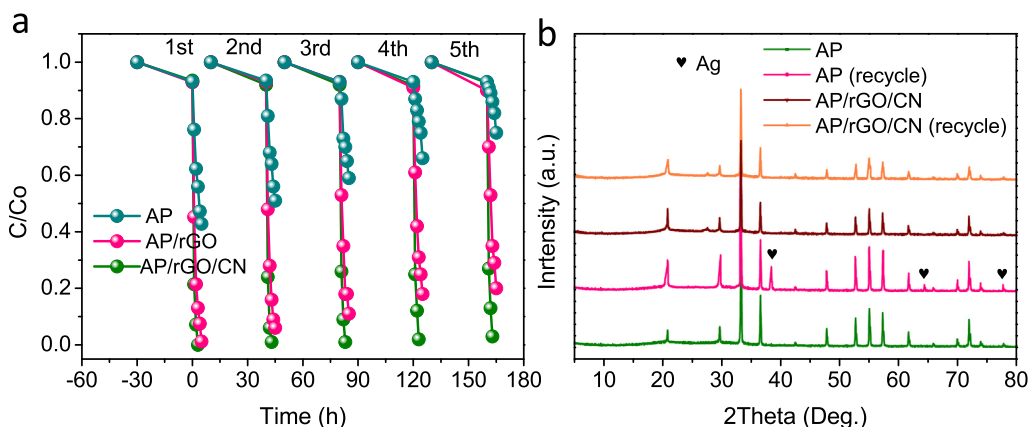
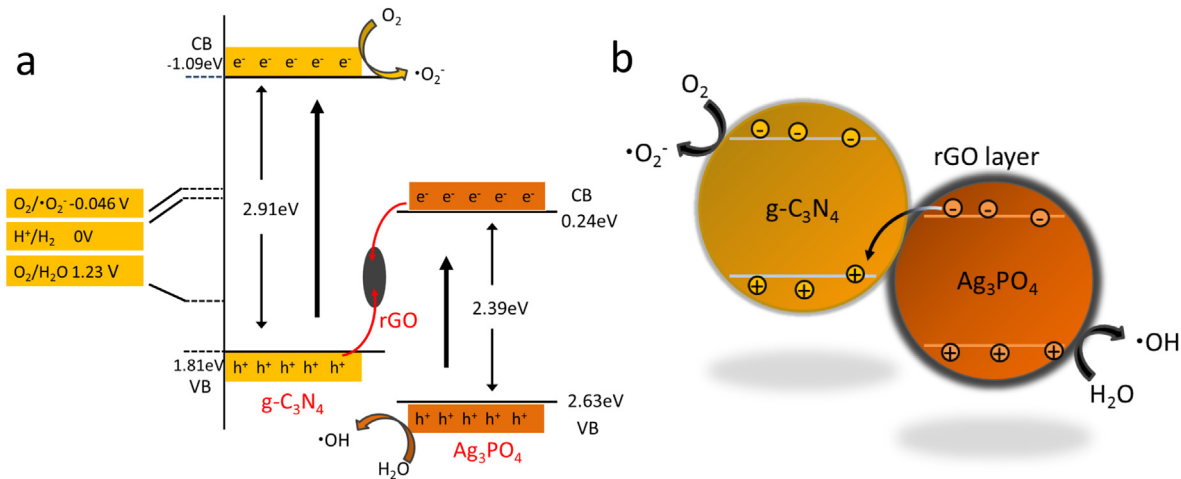


Fig. 10. (a) repeated photocatalytic experiments of AP, AP/rGO, and AP/rGO/CN composite; (b) XRD patterns of AP and AP/rGO/CN composite after 5 runs.

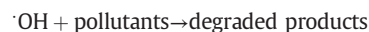
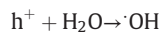
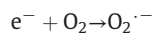


Scheme 1. (a) the photocatalytic degradation mechanism of pollutants; (b) Photocorrosion-inhibition mechanism.

3.5. Possible photocatalytic mechanism

RhB was chosen as the target pollutant in the trapping experiments to investigate the main active species in the photocatalytic degradation process. Fig. 11 shows that only benzoquinone (BQ, scavenger of $O_2^{\cdot-}$) and EDTA-2Na (scavenger of h^+) have obvious influence on the degradation efficiency towards RhB for AP/rGO, and the photocatalytic reaction was almost completely inhibited in the presence of EDTA-2Na. The photodegradation efficiency showed no obvious reduction after the addition of isopropanol (IPA, scavenger of $\cdot OH$). The degradation rate of RhB declined from 0.791 to 0.712, 0.514 and 0.06 min^{-1} , with the addition of BQ, IPA and EDTA-2Na, respectively (Wang et al., 2018). The above results demonstrated that the h^+ and $O_2^{\cdot-}$ are the main active species for AP photocatalysis. However, for AP/rGO/CN, the photodegradation could all be obviously deactivated in the presence of BQ, IPA and EDTA-2Na, and the degradation rate of RhB declined from 1.08 to 0.756, 0.116, and 0.21 min^{-1} , respectively, suggesting that all three active species ($O_2^{\cdot-}$, h^+ and $\cdot OH$) worked well in the photocatalytic process for AP/rGO/CN composite. Clearly, the holes can enrich on the VB of AP/rGO/CN (thereby retaining sufficient capacity to oxidize H_2O species to $\cdot OH$) only when the electron and holes in AP/rGO/CN migrate by the Z-scheme mechanism.

Therefore, the photocatalytic degradation mechanism of pollutants is shown as follow:



And the detailed photocatalytic degradation mechanism is also shown in Scheme 1a. Fig. 12 shows the steady-state PL spectra of pure AP and AP hybrid nanocomposites. The lower PL intensity means the lower recombination possibility of photo-generated charge carriers. Pure AP exhibited strong emission peak at around 525 nm and a shoulder at 460 nm. It can be seen that AP/CN, AP/GO, and AP/rGO/CN showed lower intensity of emission spectra than that of AP, and the PL intensity of AP/rGO/CN is the lowest. The above results indicate that the AP/rGO/CN have a relatively high carrier separation efficiency.

3.6. Anti-photocorrosion mechanism

Photocorrosion phenomenon occurs quite commonly on silver phosphate-based photocatalysts which significantly limits their practical applications. Herein, silver phosphate-based Z-Scheme photocatalytic system was proposed to inhibit the photocorrosion. Scheme 1b illustrates photoinduced e^- in the CB of AP migrate to the VB of CN rapidly via rGO and then combined with the holes in the VB of CN timely, which may effectively reduce their opportunities to react with Ag^+ , thus inhibiting the photocorrosion to an extent. More importantly, the photoinduced holes could aggregate on AP and form a rich-hole region (Li et al., 2017; Yu et al., 2016a, 2016b). Herein, rGO not only plays the role of interparticle electron mediator but also acts as sheltering layer which can also protect AP from photocorrosion. Hence, the efficient AP/rGO/CN Z-Scheme photocatalytic system was synthesized and it was demonstrated that Z-Scheme photocatalytic system effectively restrains the photocorrosion of AP because of the unique electron transfer paths and the synergistic effect of each component. This strategy efficiently deals with photocorrosion phenomenon of AP and can be applied to other photosensitive semiconductors.

4. Conclusions

A stable Z-scheme photocatalytic system for efficiently removing antibiotics from water has been successfully constructed. A novel ternary

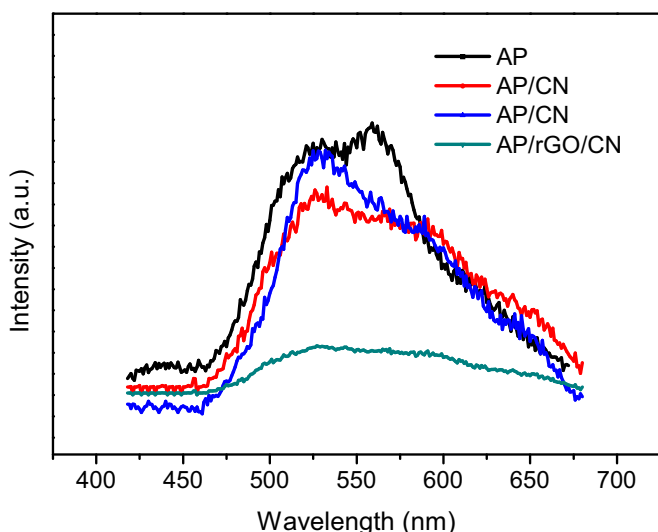


Fig. 12. PL spectra of AP and AP hybrid materials.

AP/rGO/CN composite was successfully fabricated via a facile chemical precipitation method at ambient conditions. The ternary AP/rGO/CN composite displayed superior photocatalytic activity towards NOF degradation under natural solar light irradiation and it also shows excellent anti-photo corrosion performance under intense outdoor light irradiation. The degradation rate of NOF over AP/rGO/CN ternary nanocomposite was 0.122 min^{-1} , which was about 4.2 folds as that of AP, respectively. Z-Scheme photocatalytic system, effective charge separation, and enhanced full spectrum-light absorption could be responsible for the improvement of photoactivity for ternary AP/rGO/CN composite. According to active species trapping experiment, $\text{O}_2^{\bullet-}$, h^+ and $\bullet\text{OH}$ were demonstrated to be the predominant radicals participating in the photodegradation induced by AP/rGO/CN composite. In addition, the introduction of rGO and CN could effectively boost the anti-photocorrosion properties of bare AP. This work provides a new application of Z-Scheme photocatalytic system for effective elimination of antibiotic pollutants under the natural light irradiation.

Supplementary data to this article can be found online at <https://doi.org/10.1016/j.scitotenv.2018.05.258>.

Acknowledgement

The study was financially supported by Projects 51579096, 51521006, 51222805, 51508175 and 51409024 supported by National Natural Science Foundation of China, the Key Research and Development Program of Hunan Province of China (2017SK2241), the National Program for Support of Top-Notch Young Professionals of China (2012).

References

- Ao, Wang, P., Wang, C., et al., 2013. Preparation of graphene oxide- Ag_3PO_4 composite photocatalyst with high visible light photocatalytic activity. *Appl. Surf. Sci.* 271 (2013), 265–270.
- Bi, Ouyang, S., Umezawa, N., Cao, J., Ye, J., et al., 2011. Facet effect of single-crystalline Ag_3PO_4 sub-microcrystals on photocatalytic properties. *J. Am. Chem. Soc.* 133 (2011), 6490–6492.
- Brown, Kulis, J., Thomson, B., Chapman, T.H., Mawhinney, D.B., et al., 2006. Occurrence of antibiotics in hospital, residential, and dairy effluent, municipal wastewater, and the Rio Grande in New Mexico. *Sci. Total Environ.* 366 (2006), 772–783.
- Cai, Liu, Y., Wang, L., Zhang, S., Zeng, Y., Yuan, J., et al., 2017. Silver phosphate-based Z-scheme photocatalytic system with superior sunlight photocatalytic activities and anti-photocorrosion performance. *Appl. Catal. B Environ.* 208 (2017), 1–13.
- Chai, Ding, J., Wang, L., Liu, Q., Ren, J., Dai, W.L., et al., 2015. Enormous enhancement in photocatalytic performance of $\text{Ag}_3\text{PO}_4/\text{HAp}$ composite: a Z-scheme mechanism insight. *Appl. Catal. B Environ.* 179 (2015), 29–36.
- Chen, Wang, W., Zhang, Z., Fang, X., et al., 2013. High-efficiency visible-light-driven $\text{Ag}_3\text{PO}_4/\text{AgI}$ photocatalysts: Z-scheme photocatalytic mechanism for their enhanced photocatalytic activity. *J. Phys. Chem. C* 117 (2013), 19346–19352.
- Chen, Yang, Q., Wang, S., Yao, F., Sun, J., Wang, Y., et al., 2017. Graphene oxide and carbon nitride nanosheets co-modified silver chromate nanoparticles with enhanced visible-light photoactivity and anti-photocorrosion performance towards multiple refractory pollutants degradation. *Appl. Catal. B Environ.* 209 (2017), 493–505.
- Deng, Tang, L., Zeng, G., Wang, J., Zhou, Y., Wang, J., et al., 2016. Facile fabrication of a direct Z-scheme $\text{Ag}_2\text{CrO}_4/\text{g-C}_3\text{N}_4$ photocatalyst with enhanced visible light photocatalytic activity. *J. Mol. Catal. A Chem.* 421 (2016), 209–221.
- Deng, Tang, L., Zeng, G., Feng, C., Dong, H., Wang, J., et al., 2017a. Plasmonic resonance excited dual Z-scheme $\text{BiVO}_4/\text{Ag}/\text{Cu}_2\text{O}$ nanocomposite: synthesis and mechanism for enhanced photocatalytic performance in recalcitrant antibiotic degradation. *Environ. Sci.: Nano* 4 (2017), 1494–1511.
- Deng, Tang, L., Zeng, G., Zhu, Z., Yan, M., Zhou, Y., et al., 2017b. Insight into highly efficient simultaneous photocatalytic removal of Cr(VI) and 2,4-dichlorophenol under visible light irradiation by phosphorus doped porous ultrathin $\text{g-C}_3\text{N}_4$ nanosheets from aqueous media: performance and reaction mechanism. *Appl. Catal. B Environ.* 203 (2017), 343–354.
- Guan, Guo, L., 2014. Cocatalytic effect of SrTiO_3 on Ag_3PO_4 toward enhanced photocatalytic water oxidation. *ACS Catal.* 4 (2014), 3020–3026.
- Guo, Ouyang, S., Zhou, H., Kako, T., Ye, J., et al., 2013. $\text{Ag}_3\text{PO}_4/\text{In}(\text{OH})_3$ composite photocatalysts with adjustable surface-electric property for efficient photodegradation of organic dyes under simulated solar-light irradiation. *J. Phys. Chem. C* 117 (2013), 17716–17724.
- He, Zhang, L., Teng, B., Fan, M., et al., 2014. New application of Z-scheme $\text{Ag}_3\text{PO}_4/\text{g-C}_3\text{N}_4$ composite in converting CO_2 to fuel. *Environ. Sci. Technol.* 49 (2014), 649–656.
- Hoffmann, Martin, S.T., Choi, W., Bahnemann, D.W., et al., 1995. Environmental applications of semiconductor photocatalysis. *Chem. Rev.* 95 (1995), 69–96.
- Hou, Zuo, F., Ma, Q., Wang, C., Bartels, L., Feng, P., et al., 2012. Ag_3PO_4 oxygen evolution photocatalyst employing synergistic action of Ag/AgBr nanoparticles and graphene sheets. *J. Phys. Chem. C* 116 (2012), 20132–20139.
- Hua, Teng, F., Zhao, Y., Xu, J., Xu, C., Yang, Y., et al., 2015. A new application of high-efficient silver salts-based photocatalyst under natural indoor weak light for wastewater cleaning. *Water Res.* 81 (2015), 366–374.
- Krumperman, et al., 1983. Multiple antibiotic resistance indexing of *Escherichia coli* to identify high-risk sources of fecal contamination of foods. *Appl. Environ. Microbiol.* 1983 (46), 165–170.
- Li, Zhang, P., Lv, R., Lu, J., Wang, T., Wang, S., et al., 2013. Selective deposition of Ag_3PO_4 on monoclinic BiVO_4 (040) for highly efficient photocatalysis. *Small* 9 (2013), 3951–3956.
- Li, Zhan, G.M., Yu, Y., Zhang, L.Z., et al., 2016. Superior visible light hydrogen evolution of Janus bilayer junctions via atomic-level charge flow steering. *Nat. Commun.* 7 (2016), 11480.
- Li, Zhang, L.X., Fan, X.Q., Wu, M.Y., Wang, M., Cheng, R.L., et al., 2017. Core-shell $\text{LaPO}_4/\text{g-C}_3\text{N}_4$ nanowires for highly active and selective CO_2 reduction. *Appl. Catal. B Environ.* 201 (2017), 629–635.
- Liu, Qi, Y., Lu, J., Lin, S., An, W., Liang, Y., et al., 2016. A stable $\text{Ag}_3\text{PO}_4/\text{g-C}_3\text{N}_4$ hybrid core@shell composite with enhanced visible light photocatalytic degradation. *Appl. Catal. B Environ.* 183 (2016), 133–141.
- Mai, Xu, L., Gao, Q., Han, C., Hu, B., Pi, Y., et al., 2010. Single $\beta\text{-AgVO}_3$ nanowire H_2S sensor. *Nano Lett.* 10 (2010), 2604–2608.
- Schneider, et al., Matsuoka, M., Takeuchi, M., Zhang, J., Horiuchi, Y., Anpo, M., et al., 2014. Understanding TiO_2 photocatalysis: mechanisms and materials. *Chem. Rev.* 114 (2014), 9919–9986.
- Sun, Gao, S., Lei, F., Xiao, C., Xie, Y., et al., 2015. Ultrathin two-dimensional inorganic materials: new opportunities for solid state nanochemistry. *Acc. Chem. Res.* 48 (2015), 3–12.
- Tada, Mitsui, T., Kiyonaga, T., Akita, T., Tanaka, K., et al., 2006. All-solid-state Z-scheme in CdS-Au-TiO_2 three-component nanojunction system. *Nat. Mater.* 5 (2006), 782.
- Tang, Zeng, G.M., Shen, G.L., Li, Y.P., Zhang, Y., Huang, D.L., et al., 2008. Rapid detection of picloram in agricultural field samples using a disposable immunomembrane-based electrochemical sensor. *Environ. Sci. Technol.* 42 (2008), 1207–1212.
- Tang, Wang, J., Zeng, G., et al., 2016. Enhanced photocatalytic degradation of norfloxacin in aqueous Bi_2WO_6 dispersions containing nonionic surfactant under visible light irradiation. *J. Hazard. Mater.* 306 (2016), 295–304.
- Tang, Fu, Y., Chang, S., et al., 2017. Construction of $\text{Ag}_3\text{PO}_4/\text{Ag}_2\text{MoO}_4$ Z-scheme heterogeneous photocatalyst for the remediation of organic pollutants. *Chin. J. Catal.* 38 (2017), 337–347.
- Teng, Liu, Z., Zhang, A., Li, M., et al., 2015. Photocatalytic performances of Ag_3PO_4 polytops for degradation of dye pollutant under natural indoor weak light irradiation. *Environ. Sci. Technol.* 49, 9489–9494.
- Voiry, Salehi, M., Silva, R., Fujita, T., Chen, M.W., Asefa, T., et al., 2013. Conducting MoS_2 Nanosheets as catalysts for hydrogen evolution reaction. *Nano Lett.* 13 (2013), 6222–6227.
- Wan, Du, X., Liu, E., Hu, Y., Fan, J., Hu, X., et al., 2017. Z-scheme visible-light-driven Ag_3PO_4 nanoparticle@ MoS_2 quantum dot/few-layered MoS_2 nanosheet heterostructures with high efficiency and stability for photocatalytic selective oxidation. *J. Catal.* 345 (2017), 281–294.
- Wang, He, L., Wang, L., Hu, P., Guo, L., Han, X., et al., 2012. Facile synthesis of Ag_3PO_4 tetrapod microcrystals with an increased percentage of exposed {110} facets and highly efficient photocatalytic properties. *CrystEngComm* 14 (2012), 8342–8344.
- Wang, Yuan, X., Wang, H., Chen, X., Wu, Z., Jiang, L., et al., 2016a. Facile synthesis of Sb_2S_3 /ultrathin $\text{g-C}_3\text{N}_4$ sheets heterostructures embedded with $\text{g-C}_3\text{N}_4$ quantum dots with enhanced NIR-light photocatalytic performance. *Appl. Catal. B Environ.* 193 (2016), 36–46.
- Wang, Tang, L., Zeng, G., Liu, Y., Zhou, Y., Deng, Y., et al., 2016b. Plasmonic Bi metal deposition and $\text{g-C}_3\text{N}_4$ coating on Bi_2WO_6 microspheres for efficient visible-light photocatalysis. *ACS Sustain. Chem. Eng.* 5 (2016), 1062–1072.
- Wang, Tang, L., Zeng, G., et al., 2017a. Atomic scale $\text{g-C}_3\text{N}_4/\text{Bi}_2\text{WO}_6$ 2D/2D heterojunction with enhanced photocatalytic degradation of ibuprofen under visible light irradiation. *Appl. Catal. B Environ.* 209 (2017), 285–294.
- Wang, Yuan, X., Wu, Y., Zeng, G., Tu, W., Sheng, C., et al., 2017b. Plasmonic Bi nanoparticles and BiOCl sheets as cocatalyst deposited on perovskite-type $\text{ZnSn}(\text{OH})_6$ microparticle with facet-oriented polyhedron for improved visible-light-driven photocatalysis. *Appl. Catal. B Environ.* 209 (2017), 543–553.
- Wang, Tang, L., Zeng, G., et al., 2018. 0D/2D interface engineering of carbon quantum dots modified Bi_2WO_6 ultrathin nanosheets with enhanced photoactivity for full spectrum light utilization and mechanism insight. *Appl. Catal. B Environ.* 222 (2018), 115–123.
- Watkinson, Murby, E., Kolpin, D., Costanzo, S., et al., 2009. The occurrence of antibiotics in an urban watershed: from wastewater to drinking water. *Sci. Total Environ.* 407 (2009), 2711–2723.
- Wen, Niu, C.G., Zhang, L., Huang, D.W., Zeng, G.M., et al., 2017. In-situ synthesis of visible-light-driven plasmonic Ag/AgCl-CdWO_4 photocatalyst. *Ceram. Int.* 43 (2017), 1922–1929.
- Wong, Jelacic, S., Habeeb, R.L., Watkins, S.L., Tarr, P.I., et al., 2000. The risk of the hemolytic-uremic syndrome after antibiotic treatment of *Escherichia coli* O157: H7 infections. *N. Engl. J. Med.* 342 (2000), 1930–1936.
- Yang, Cui, H., Li, Y., Qin, J., Zhang, R., Tang, H., et al., 2013. Fabrication of Ag_3PO_4 -graphene composites with highly efficient and stable visible light photocatalytic performance. *ACS Catal.* 3 (2013), 363–369.
- Yao, Zhang, B., Huang, C., Ma, C., Song, X., Xu, Q., et al., 2012. Synthesis and characterization of high efficiency and stable $\text{Ag}_3\text{PO}_4/\text{TiO}_2$ visible light photocatalyst for the degradation of methylene blue and rhodamine B solutions. *J. Mater. Chem.* 22 (2012), 4050–4055.
- Ye, Liu, J., Gong, C., Tian, L., Peng, T., Zan, L., et al., 2012. Two different roles of metallic Ag on Ag/AgX/BiOX ($X = \text{Cl, Br}$) visible light photocatalysts: surface plasmon resonance and Z-scheme bridge. *ACS Catal.* 2 (2012), 1677–1683.

- Yi, Ye, J., Kikugawa, N., Kako, T., Ouyang, S., Stuart-Williams, H., et al., 2010. An orthophosphate semiconductor with photooxidation properties under visible-light irradiation. *Nat. Mater.* 9 (2010), 559.
- Yu, Li, G., Kumar, S., Yang, K., Jin, R., et al., 2014. Phase transformation synthesis of novel $\text{Ag}_2\text{O}/\text{Ag}_2\text{CO}_3$ heterostructures with high visible light efficiency in photocatalytic degradation of pollutants. *Adv. Mater.* 26 (2014), 892–898.
- Yu, Chen, W., Wang, X., et al., 2016a. Enhanced photocatalytic activity and photoinduced stability of Ag-based photocatalysts: the synergistic action of amorphous-Ti (IV) and Fe (III) cocatalysts. *Appl. Catal. B Environ.* 187 (2016), 163–170.
- Yu, Shang, L., Bian, T., Shi, R., Waterhouse, G.I., Zhao, Y., et al., 2016b. Nitrogen-doped porous carbon nanosheets templated from $g\text{-C}_3\text{N}_4$ as metal-free electrocatalysts for efficient oxygen reduction reaction. *Adv. Mater.* 25 (2016), 5080–5086.
- Zeng, Chen, M., Zeng, Z., et al., 2013. Risks of neonicotinoid pesticides. *Science* 340 (2013), 1403.
- Zhang, Lai, C., Zeng, G., Huang, D., Yang, C., Wang, Y., et al., 2016. Efficacy of carbonaceous nanocomposites for sorbing ionizable antibiotic sulfamethazine from aqueous solution. *Water Res.* 95 (2016), 103–112.
- Zhou, Yu, J., Jaroniec, M., et al., 2014. All-solid-state Z-scheme photocatalytic systems. *Adv. Mater.* 26 (2014), 4920–4935.